Light-Front Interpretation of Proton Generalized Polarizabilities

M. Gorchtein,[1] C. Lorcé,[2] B. Pasquini,[3] and M. Vanderhaeghen[2]
[1]Indiana University, Bloomington, Indiana 47408, USA
[2]Institut für Kernphysik, Mainz Universität, 55099 Mainz, Germany
[3]Dipartimento di Fisica Nucleare e Teorica, Università di Pavia, and Istituto Nazionale di Fisica Nucleare, Sezione di Pavia, I-27100 Pavia, Italy
(Received 15 November 2009; published 15 March 2010)

We extend the recently developed formalism to extract light-front quark charge densities from nucleon form factor data to the deformations of these quark charge densities when applying an external electric field. We show that the resulting induced polarizations can be extracted from proton generalized polarizabilities. The available data for the generalized electric polarizability of the proton yield a pronounced structure in its induced polarization at large transverse distances, which will be pinned down by forthcoming high precision virtual Compton scattering experiments.

DOI: 10.1103/PhysRevLett.104.112001 PACS numbers: 13.60.Fz, 14.20.Dh

The distribution of charge is a basic quantity which characterizes a many-body system. In the case of relativistic many-body systems such as hadrons, composed of near massless quarks, a field theoretic consistent charge density can be formulated by considering the system in a light-front frame. In such a frame, the pair creation by the probing photon is suppressed, and the photon only couples to forward moving quarks, allowing for a density interpretation. Such a charge density interpretation, based on elastic form factor data, was recently given for the nucleon [1,2], for spin-1 systems [3], spin-3/2 systems [4], and extended to higher spin systems in [5].

Any charge density will deform when subjected to an external electric field and develop an induced polarization. The quantity describing the ''ease'' by which such distribution will deform is referred to as the electric polarizability. In this work we will extend the formalism of light-front charge densities to obtain the spatial deformations of these densities. We will show that the resulting induced polarizations can be obtained from nucleon generalized polarizabilities (GPs) [6,7], which have been measured in recent years by precision virtual Compton scattering (VCS) experiments; see Refs. [8,9] for reviews.

We consider the VCS process on the nucleon $\gamma^*(q) + N(p) \to \gamma(q') + N(p')$. Its kinematics are described in terms of Lorentz scalars: $Q^2 = -q^2$, $\nu \equiv q \cdot P/M$, with $P = (p + p')/2$, and $t = (p - p')^2$. The dynamical information which is accessed in the VCS process is described by the matrix element of a time-ordered product of two electromagnetic (e.m.) current operators as

$$H^{\mu\nu} = -i \int d^4x e^{-iq\cdot x} \langle p', \lambda'_N | T[J^\mu(x), J^\nu(0)] | p, \lambda_N \rangle, \quad (1)$$

with λ_N (λ'_N) the helicities of the initial (final) nucleons. In this work, we consider the VCS tensor in the low-energy limit, $q' \to 0$. In such a limit, the final soft photon plays the role of an applied quasistatic electromagnetic field, and the VCS process measures the linear response of the nucleon to this applied field [6,8]. This linear response can be parameterized through six Q^2 dependent GPs, denoted by $P^{(\rho' l', \rho l) S}$ [6,7]. In this notation, ρ (ρ') refers to the Coulomb-electric (L), or magnetic (M) nature of the initial (final) photon, l ($l' = 1$) is the angular momentum of the initial (final) photon, and S differentiates between the spin-flip ($S = 1$) and non spin-flip ($S = 0$) transition at the nucleon side.

To arrive at a spatial representation of the information contained in the GPs, we consider the process in a symmetric light-front frame, denoting the average direction of the fast moving protons as the z axis. We indicate the (large) light front + component by P^+ (defining $a^\pm \equiv a^0 \pm a^3$), and choose the symmetric frame by requiring that $\Delta = p' - p$ is purely transversal, i.e., $\Delta^+ = 0$. To access the GPs, we can restrict ourselves to the terms in the VCS tensor that are linear in the outgoing photon energy (proportional to ν), along the line $t = -Q^2$. In this limit the light-front kinematics is given by $P^\mu = (P^+/2)\bar{n}^\mu + M^2(1 + \tau)/(2P^+)n^\mu$, $\Delta^\mu = q^\mu_\perp$, $q^\mu = (\eta P^+)\bar{n}^\mu + q^\mu_\perp$, $q'^\mu = (\eta P^+)\bar{n}^\mu$, with lightlike vectors $\bar{n} = (1, 0, 0, 1)$, $n = (1, 0, 0, -1)$. Furthermore, the two transverse components of the virtual photon momentum are denoted by $\vec{q}_\perp$ with $Q^2 = \vec{q}^2_\perp$, and $\tau \equiv Q^2/(4M^2)$, with M the nucleon mass. The (small) momentum fraction η is obtained as $\eta = \nu/(M(1 + \tau))$.

In the light-front frame, the + component of the current J^μ in (1) is a positive definite operator for each quark flavor, allowing for a light-front charge density interpretation. The VCS light-front helicity amplitudes can then be obtained from the VCS tensor $H^{\mu\nu}$ as

$$H(\lambda'_\gamma, \lambda'_N, \lambda_N) \equiv \varepsilon'^*_\nu(\lambda'_\gamma) H^{+\nu}, \quad (2)$$

with transverse outgoing photon polarization vector denoted by $\vec{\epsilon}'_\perp$, and $\lambda'_\gamma = \pm 1$ denoting its helicity. In the following, we will consider the polarization component of the outgoing photon corresponding with an electric field, $\vec{E} = -\partial \vec{A}/\partial t$, which can be expressed as

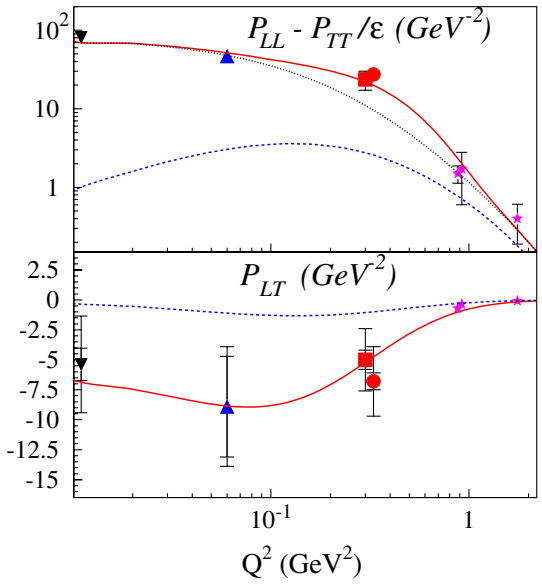

FIG. 1 (color online). Structure functions describing unpolarized VCS on a proton compared with data from MAMI (circles [14], squares [15]), MIT-Bates (up triangles [16]), and JLab (stars [17]). The RCS data [13] are shown by the (black) down triangles (slightly displaced in Q^2). The curves are based on the parameterizations of Eqs. (10) and (11) for the proton GPs, and are shown for $\varepsilon = 0.645$. Upper panel: dotted (black) curve for $\Lambda_\alpha = 0.7$ GeV, $C_\alpha = 0$ (GP I); solid (red) curve for $\Lambda_\alpha = 0.7$ GeV, $C_\alpha = -150$ GeV^{-7} (GP II). Lower panel: solid (red) curve for $\Lambda_\beta = 0.5$ GeV. The dashed (blue) curves in both panels show the spin GP contributions.

$$\vec{E} \sim iq'^0 \vec{\epsilon}'_\perp = i\frac{\nu}{(1+\tau)}\frac{P^+}{M}\vec{\epsilon}'_\perp. \tag{3}$$

Any system of charges will respond to such an applied electric field, resulting in an induced polarization $\vec{P}_0$, which will be forced to align with the applied electric field such as to minimize its energy $-\vec{E}\cdot\vec{P}_0$. The linear response in q'^0 of the helicity averaged VCS amplitude therefore allows us to define an induced polarization $\vec{P}_0$ as

$$i\vec{\varepsilon}'^*_\perp(\lambda'_\gamma)\cdot\vec{P}_0 \equiv \frac{(1+\tau)}{(2P^+)}\frac{\partial}{\partial\nu}H(\lambda'_\gamma,\lambda_N,\lambda_N)|_{\nu=0}. \tag{4}$$

The induced polarization $\vec{P}_0$ for the helicity averaged case can be worked out from Eq. (2) as

$$\vec{P}_0(\vec{q}_\perp) = i\hat{q}_\perp A(Q^2), \tag{5}$$

where A can be expressed in terms of the GPs as

$$A = -(2M)\sqrt{\tau}\sqrt{\frac{3}{2}}\sqrt{\frac{1+2\tau}{1+\tau}}\Big\{-P^{(L1,L1)0} + \frac{1}{2}P^{(M1,M1)0} - \sqrt{\frac{3}{2}}P^{(L1,L1)1} - \sqrt{\frac{3}{2}}(1+\tau)[P^{(M1,M1)1} + \sqrt{2}(2M\tau)P^{(L1,M2)1}]\Big\}, \tag{6}$$

which depends on the scalar GPs, as well as those spin GPs which enter the unpolarized VCS response functions.

In an analogous way, we can define the linear response to an external quasistatic e.m. dipole field when the nucleon is in an eigenstate of transverse spin, $\vec{S}_\perp \equiv \cos\phi_S\hat{e}_x + \sin\phi_S\hat{e}_y$, with ϕ_S the angle indicating the spin vector direction. Analogously to Eq. (4), the induced polarization $\vec{P}_T$ for a state of transverse spin can be worked out from the sum of contributions from spin-averaged and spin-flip light-front helicity amplitudes as

$$\vec{P}_T(\vec{q}_\perp) = i\hat{q}_\perp A(Q^2) + \hat{q}_\perp(\vec{S}_\perp\times\vec{e}_z)\cdot\hat{q}_\perp B(Q^2) + (\vec{S}_\perp\times\vec{e}_z)C(Q^2). \tag{7}$$

The functions B and C entering the induced polarization $\vec{P}_T$ can be expressed in terms of the GPs as

$$B = -(2M)\tau\sqrt{\frac{3}{2}}\sqrt{\frac{1+2\tau}{1+\tau}}\Big\{P^{(L1,L1)0} - \frac{1}{2}P^{(M1,M1)0} + \sqrt{\frac{3}{2}}\Big[-\sqrt{2}(2M)(1+\tau)P^{(L1,M2)1} + P^{(L1,L1)1} + \sqrt{\frac{3}{2}}(2M)(1+\tau)P^{(M1,L2)1}\Big]\Big\}, \tag{8}$$

$$C = (2M)(1+\tau)\frac{3}{2}\sqrt{\frac{1+2\tau}{1+\tau}}\Big\{P^{(M1,M1)1} + P^{(L1,L1)1} + \sqrt{\frac{3}{2}}(2M\tau)P^{(M1,L2)1}\Big\}. \tag{9}$$

To evaluate the induced polarizations, we use the available empirical information on the GPs. The four spin GPs are described, following [10], by a dispersive part, and a π^0 pole part. The dispersive part is saturated by πN intermediate states, using empirical information from pion photo- and electroproduction as encoded in the MAID2007 parameterization [11]. The electric and magnetic GPs are decomposed as a sum of a dispersive πN part and an asymptotic part. The asymptotic part of the magnetic GP is described by a dipole:

$$P^{(M1,M1)0}_{\rm asy}(Q^2) = P^{(M1,M1)0}_{\rm asy}(0)/(1+Q^2/\Lambda_\beta^2)^2. \tag{10}$$

To describe the available data for the electric GP, we allow for an asymptotic part consisting of a sum of a dipole and a Gaussian, in the same vein as the parameterization proposed in [12] for the nucleon form factors

$$P^{(L1,L1)0}_{\rm asy}(Q^2) = P^{(L1,L1)0}_{\rm asy}(0)/(1+Q^2/\Lambda_\alpha^2)^2 + C_\alpha Q^4 e^{-(Q^2-0.15)/0.15}. \tag{11}$$

The values at the real photon point have been fixed as the difference between the empirical information for the proton electric and magnetic polarizabilities, obtained from real Compton scattering (RCS) experiments [13], and the

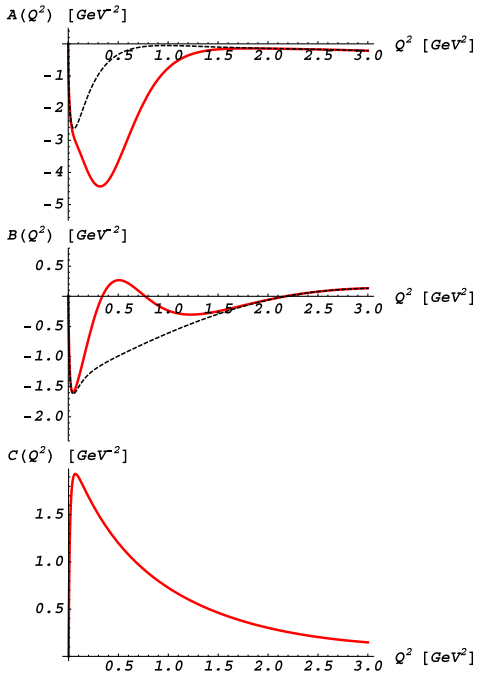

FIG. 2 (color online). Q^2 dependence of the functions A, B, and C. Dotted (black) curves are for parameterization GP I; solid (red) curves are for GP II; see caption of Fig. 1.

dispersive πN contribution, yielding $P_{\rm asy}^{(L1,L1)0}(0) = -14.37\ {\rm GeV}^{-3}$, and $P_{\rm asy}^{(M1,M1)0}(0) = 21.82\ {\rm GeV}^{-3}$. The remaining three parameters Λ_β, Λ_α, and C_α, describing the Q^2 dependence of the asymptotic parts of the spin independent GPs can be determined by a fit to available VCS data. In Fig. 1, we show the comparison with the experimentally measured unpolarized structure functions $P_{LL} - P_{TT}/\varepsilon$ (P_{LT}), proportional to the electric (magnetic) GPs,, respectively, up to a small spin GP contribution (dashed curves). For an exhaustive description of VCS observables, we refer to Refs. [8,9]. For the magnetic GP, one sees from P_{LT} on Fig. 1 that a good fit to all data is obtained for $\Lambda_\beta = 0.5$ GeV. For the electric GP, a fit to the MIT-Bates and JLab data is obtained for $C_\alpha = 0$, and $\Lambda_\alpha = 0.7$ GeV (denoted by parameterization GP I). However, this does not describe the MAMI data at intermediate Q^2, which require an additional structure, parameterized through the Gaussian term in Eq. (11). A good description of all available data is obtained for $\Lambda_\alpha = 0.7$ GeV, and $C_\alpha = -150\ {\rm GeV}^{-7}$ (denoted by parameterization GP II). The above empirical parameterizations for the GPs, allow to evaluate the Q^2 dependence of A, B, and C, as displayed in Fig. 2. One clearly notices the enhancement in A as well as the structure at intermediate Q^2 values in B in GP II.

The light-front frame allows us to use this empirical information to visualize the deformation of the charge densities in an external e.m. field and map out the transverse position space dependence of the induced polarization. For the case of a nucleon in a state of definite helicity, the transverse position space dependence of the induced polarization $\vec{P}_0$ is given by

$$\vec{P}_0(\vec{b}) = \int \frac{d^2\vec{q}_\perp}{(2\pi)^2} e^{-i\vec{q}_\perp\cdot\vec{b}} \vec{P}_0(\vec{q}_\perp), \tag{12}$$

which can be worked out using Eq. (5) as

$$\vec{P}_0(\vec{b}) = \hat{b} \int_0^\infty \frac{dQ}{(2\pi)} Q J_1(bQ) A(Q^2), \tag{13}$$

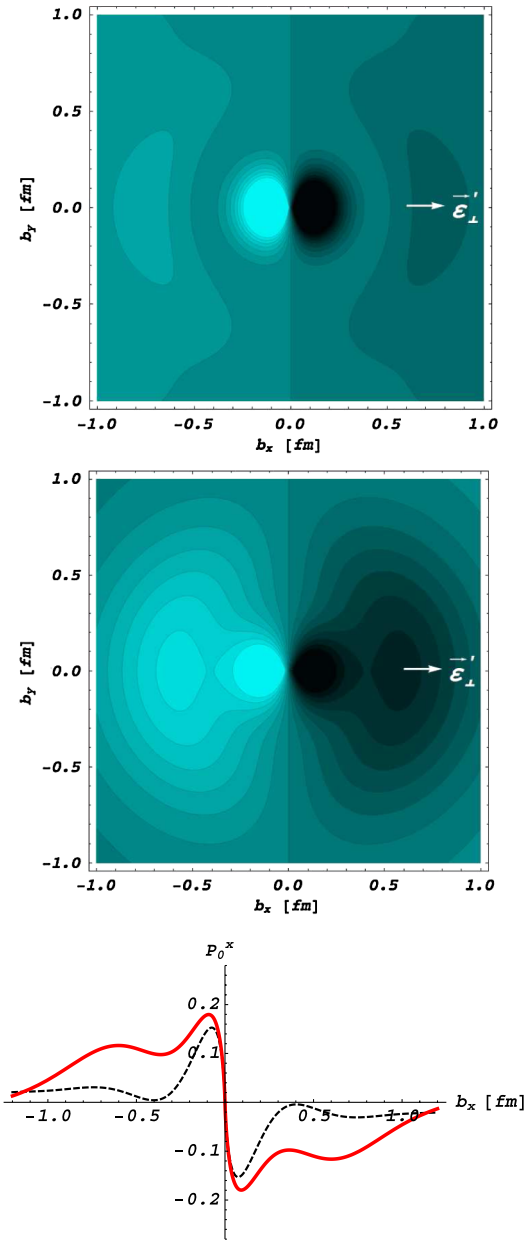

FIG. 3 (color online). Induced polarization, P_0^x, in a proton of definite light-cone helicity, when submitted to an e.m. field with photon polarization along the x axis, as indicated. Upper (middle) panel is for GP I (GP II); see caption of Fig. 1. The light (dark) regions correspond to the largest (smallest) values. The lower panel compares P_0^x along $b_y = 0$: dotted curve is for GP I; solid curve is for GP II.

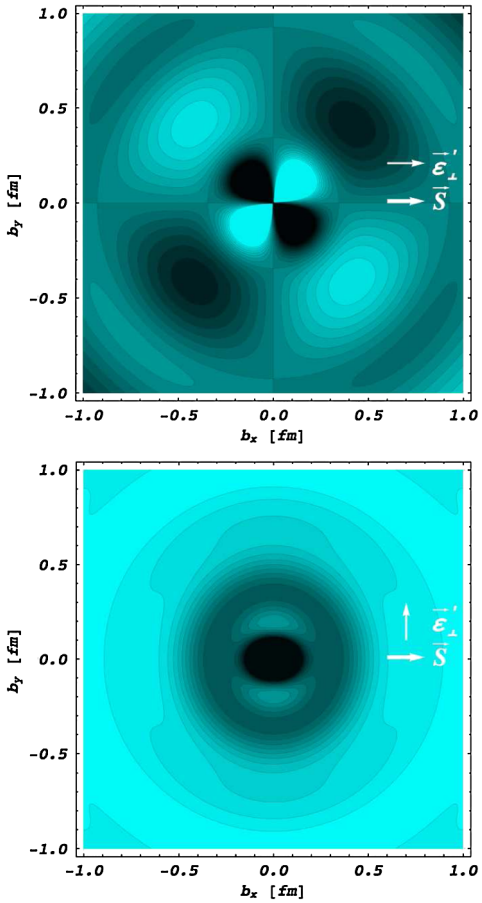

FIG. 4 (color online). Induced polarization density in a proton, with spin $\vec{S}$ oriented along the x-axis, when submitted to an e.m. field. The upper (lower) panels are for $P_T^x - P_0^x$ ($P_T^y - P_0^y$), respectively, and correspond with photon polarization along the x axis (y axis) as indicated. The light (dark) regions correspond to the largest (smallest) values using parameterization GP II.

where $\vec{b}$ is the transverse position, $b = |\vec{b}|$, and $\hat{b} = \vec{b}/b$.

The dipole pattern described by Eq. (13) is shown in Fig. 3. One clearly sees that the enhancement at intermediate Q^2 in the electric GP (upper panel in Fig. 1) in GP II, as compared with GP I, yields a spatial distribution of the induced polarization that extends noticeably to larger transverse distances. Forthcoming VCS experiments, that are conceived to pin down more precisely the behavior of the GPs at intermediate Q^2 values, will therefore be able to verify this large distance structure.

For the case of a nucleon in an eigenstate of transverse spin, the transverse position dependence of the induced polarization $\vec{P}_T$ can likewise be worked out as

$$\vec{P}_T(\vec{b}) = \vec{P}_0(\vec{b}) - \hat{b}(\vec{S}_\perp \times \vec{e}_z) \cdot \hat{b} \int_0^\infty \frac{dQ}{(2\pi)} Q J_2(bQ) B + (\vec{S}_\perp \times \vec{e}_z) \int_0^\infty \frac{dQ}{(2\pi)} Q \left[J_0(bQ) C + \frac{J_1(bQ)}{bQ} B \right], \tag{14}$$

displaying dipole, quadrupole, and monopole patterns. In Fig. 4 we show the spatial distributions in the induced polarization for a proton of transverse spin (chosen along the x axis) for parameterization GP II. The component $P_T^x - P_0^x$ displays a quadrupole pattern with pronounced strength around 0.5 fm due to the electric GP, whereas the component $P_T^y - P_0^y$ shows in addition a monopole pattern, dominated by the π^0 pole contribution.

In summary, in this work we have used recent data on proton GPs to map out the spatial dependence of the induced polarizations in an external e.m. field. The formalism to extract in a field theoretic consistent way light-front densities from nucleon form factor data has been extended in this work to the deformations of these quark charge densities when applying an external e.m. field. It has been shown that the available proton electric GP data yield a pronounced structure in its induced polarization at large transverse distances of 0.5–1 fm. At Q^2 values smaller than 0.1 GeV^2, chiral effective field theory was found to well describe the VCS data, highlighting the role of pions in the nucleon structure. Such description can however not be applied at intermediate and large Q^2 values. This transition region is dominated by nucleon resonance structure, which can be described by dispersion relations. Forthcoming VCS precision experiments at MAMI in this intermediate Q^2 region, will be able to better determine this structure, thus complementing our picture of the distribution of quark charges in the nucleon as obtained through elastic form factors.

[1] G. A. Miller, Phys. Rev. Lett. **99**, 112001 (2007).
[2] C. E. Carlson and M. Vanderhaeghen, Phys. Rev. Lett. **100**, 032004 (2008).
[3] C. E. Carlson and M. Vanderhaeghen, Eur. Phys. J. A **41**, 1 (2009).
[4] C. Alexandrou *et al.*, Nucl. Phys. **A825**, 115 (2009).
[5] C. Lorce, Phys. Rev. D **79**, 113011 (2009).
[6] P. A. M. Guichon, G. Q. Liu, and A. W. Thomas, Nucl. Phys. **A591**, 606 (1995).
[7] D. Drechsel, G. Knochlein, A. Y. Korchin, A. Metz, and S. Scherer, Phys. Rev. C **57**, 941 (1998); **58**, 1751 (1998).
[8] P. A. M. Guichon and M. Vanderhaeghen, Prog. Part. Nucl. Phys. **41**, 125 (1998).
[9] D. Drechsel, B. Pasquini, and M. Vanderhaeghen, Phys. Rep. **378**, 99 (2003).
[10] B. Pasquini, D. Drechsel, M. Gorchtein, A. Metz, and M. Vanderhaeghen, Phys. Rev. C **62**, 052201(R) (2000); Eur. Phys. J. A **11**, 185 (2001).
[11] D. Drechsel, S. S. Kamalov, and L. Tiator, Eur. Phys. J. A **34**, 69 (2007).
[12] J. Friedrich and T. Walcher, Eur. Phys. J. A **17**, 607 (2003).
[13] V. Olmos de Leon *et al.*, Eur. Phys. J. A **10**, 207 (2001).
[14] J. Roche *et al.* (VCS Collaboration and A1 Collaboration), Phys. Rev. Lett. **85**, 708 (2000).
[15] P. Janssens *et al.* (A1 Coll.), Eur. Phys. J. A **37**, 1 (2008).
[16] P. Bourgeois *et al.*, Phys. Rev. Lett. **97**, 212001 (2006).
[17] G. Laveissiere *et al.* (Jefferson Lab Hall A Coll.), Phys. Rev. Lett. **93**, 122001 (2004).